

Attribute Localization and Revision Network for Zero-Shot Learning

Junzhe Xu¹, Suling Duan², Chenwei Tang¹, Zhenan He^{1*} and Jiancheng Lv¹

¹College of Computer Science, Sichuan University, China

²School of Statistics, Chengdu University of Information Technology, China

druryxu@stu.scu.edu.cn, dsl@cuit.edu.cn, {tangchenwei, zhenan, lvjiancheng}@scu.edu.cn

Abstract

Zero-shot learning enables the model to recognize unseen categories with the aid of auxiliary semantic information such as attributes. Current works proposed to detect attributes from local image regions and align extracted features with class-level semantics. In this paper, we find that the choice between local and global features is not a zero-sum game, global features can also contribute to the understanding of attributes. In addition, aligning attribute features with class-level semantics ignores potential intra-class attribute variation. To mitigate these disadvantages, we present Attribute Localization and Revision Network in this paper. First, we design Attribute Localization Module (ALM) to capture both local and global features from image regions, a novel module called Scale Control Unit is incorporated to fuse global and local representations. Second, we propose Attribute Revision Module (ARM), which generates image-level semantics by revising the ground-truth value of each attribute, compensating for performance degradation caused by ignoring intra-class variation. Finally, the output of ALM will be aligned with revised semantics produced by ARM to achieve the training process. Comprehensive experimental results on three widely used benchmarks demonstrate the effectiveness of our model in the zero-shot prediction task.

1 Introduction

Human beings have an outstanding ability to recognize objects that have never been seen before. However, traditional deep learning models generally struggle to identify classes that do not appear in the training set, which largely limits deep learning's ability to simulate human behavior. To tackle this problem, Zero-Shot Learning (ZSL) [Lampert *et al.*, 2009] has been proposed to identify images from unseen classes.

The key to ensuring the success of ZSL is the semantics of all classes provided during training, which acts as a bridge to help the model transfer knowledge from seen to unseen classes. In a typical setting [Xian *et al.*, 2018a], a semantic

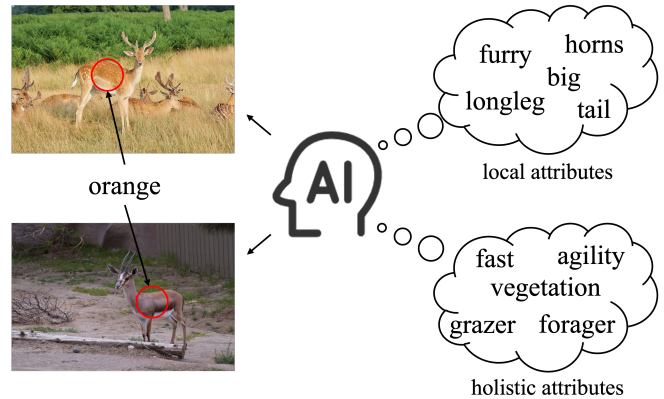


Figure 1: Two existing problems an attention-based model will encounter during training, i.e., potential attribute variation within a class (left side) and two different scales of attributes (right side).

is a vector with the value at each dimension representing the saliency value of a certain attribute, i.e., if an attribute does not present on the image, the value will be zero.

There are two mainstream ZSL settings, conventional ZSL [Lampert *et al.*, 2009] and generalized ZSL (GZSL) [Chao *et al.*, 2016]. The former assumes that all samples in the test set belong to unseen classes. However, samples belonging to seen classes may also appear during testing in real-world scenarios. Hence, GZSL has been introduced. It adds samples from seen classes into the test set, which enlarges the classification space from unseen classes to both seen and unseen classes.

In the beginning, GZSL follows the idea of conventional ZSL to leverage cross-modal projection, which aligns visual and semantic features to build a visual-semantic space, and predictions are made through the nearest neighbor algorithm. Nevertheless, since the model is fully trained on seen classes, it will be severely biased towards seen classes during testing, which tends to classify unseen samples into seen classes. Since such an overfitting problem is caused by the extreme data imbalance between seen and unseen classes, generation-based methods [Xian *et al.*, 2018b; Chen *et al.*, 2021b] proposed to directly generate unseen samples and convert the GZSL task to a fully supervised task. However, generation-based methods use the global

*Corresponding Author.

image representations extracted by a pre-trained backbone as training samples, where discriminative local information will be submerged in the global representation. To this end, attention-based methods [Xu *et al.*, 2020; Chen *et al.*, 2021a; Chen *et al.*, 2022] abandoned utilizing global features but proposed to locate and evaluate the saliency value of each attribute directly from image regions, which avoids the loss of local discriminative features.

The key to success in the attention-based method is whether it can accurately establish a one-to-one correspondence between image regions and attributes. Thus, previous works concentrate on building better local representation extractors to capture discriminative attribute information. However, there may be no clear clues in the image for building such a correspondence. To illustrate, there exist attributes that are more semantically related rather than visually related to the image. For a better understanding, the right side of Figure 1 lists a few examples of different kinds of attributes that belong to the antelope. As we can see, the visually related attributes, i.e., local attributes, clearly depict a part of the image, and semantically-related attributes, i.e., holistic attributes, are the condensation of highly abstract knowledge that cannot be captured purely by eyes. In some situations, annotating local attributes manually is hard or expensive to achieve and off-the-shelf external information, e.g., knowledge graph, provides a convenient way to annotate attributes automatically. However, such external knowledge will unavoidably bring some semantically related attributes. Therefore, it is crucial to consider the existence of holistic attributes in many real applications.

Another phenomenon that hinders the model localize attributes from the image is intra-class attribute variation, which means the same attribute will present differently in different images. We exhibit such a variation in the left side of Figure 1. Since two pictures are taken under different conditions, the attribute "orange" representation is diverse. Current attention-based methods adopted a single semantic vector as the ground truth learning target for all images in one class, which ignores the possible attribute variation. Evaluating the value of each attribute independently causes the individual attribute prediction result to have an effect on the overall result, so the attribute variation during training needs to be meticulously considered.

The above two phenomena are not well addressed in previous works, which makes them two challenges that cannot be ignored on the road of ZSL development. To alleviate these problems, we propose a novel framework called Attribute Localization and Revision Network (ALRN). We first discover the importance of global features in understanding attributes rather than purely adopting local features. Since it is unreasonable to enforce the model to detect undetectable holistic attributes, the incorporation of global features helps the model understand holistic attributes from the perspective of the entire image. Also, it can act as a complement to the attention mechanism such as deducing the attribute "horns" if we know there is an antelope in the image. Therefore, our proposed Attribute Localization Module (ALM) extracts local features through the attention mechanism and global features via average pooling. Then, we introduce Scale Control

Unit (SCU) to fuse these two kinds of features. To mitigate the problem of ignoring intra-class attribute variation, we propose the Attribute Revision Module (ARM). For each input image, it first generates a specific set of revision weights for all attributes and conducts an element-wise product between revision weights and class-level attribute values to generate new sets of image-level attribute values. To this end, ARM considers intra-class attribute variation from the perspective of learning from revised targets.

The contributions of our work are summarized as follows:

- We exploit the importance of global features in understanding attributes, and the scale control mechanism is designed to aggregate local and global features.
- Considering possible attribute variation lies among images within the same class, we propose the attribute revision mechanism to revise class-level attribute saliency value into image-level.
- The experimental results on three ZSL benchmarks demonstrate our proposed ALRN has a remarkable ability in both conventional ZSL and GZSL prediction tasks.

2 Related Works

Since samples and semantics lie on different modal spaces, projection-based methods [Chao *et al.*, 2016; Akata *et al.*, 2015a; Akata *et al.*, 2015b; Frome *et al.*, 2013] proposed to project and align them on a common space. However, after GZSL becomes the research emphasis of ZSL, projection-based methods suffer from severe bias toward seen classes. To alleviate this problem, calibrated stacking mechanism [Chao *et al.*, 2016], knowledge transfer [Jiang *et al.*, 2019; Liu *et al.*, 2018; Li *et al.*, 2019b], episode-training [Yu *et al.*, 2020] are introduced.

Another way to prevent the model from bias toward seen classes is generating unseen samples using generative models [Goodfellow *et al.*, 2014; Kingma and Welling, 2014], where researchers [Narayan *et al.*, 2020; Xian *et al.*, 2019; Xian *et al.*, 2018b; Mishra *et al.*, 2018; Verma *et al.*, 2018] build a generator with semantics as conditional information. To promote the quality of generated samples, some works try to learn the detailed distribution of seen samples [Li *et al.*, 2019a; Xie *et al.*, 2022], incorporate the distribution of semantics into the learning process [Vyas *et al.*, 2020; Tang *et al.*, 2022], and add distribution regulation to synthesized seen samples [Han *et al.*, 2020; Han *et al.*, 2021].

Besides projection and generation methods, researchers have turned their sights to directly localizing attributes on images in recent years. Along this line, attention mechanism [Huynh and Elhamifar, 2020; Chen *et al.*, 2022; Chen *et al.*, 2021a; Liu *et al.*, 2021; Liu *et al.*, 2019; Xie *et al.*, 2019], max pooling [Yang *et al.*, 2021; Xu *et al.*, 2020] are exploited to capture attributes from the feature map produced by a backbone.

Several works propose image-adaptive semantics [Liu *et al.*, 2019; Chou *et al.*, 2020] in order to solve the performance degradation brought by semantic ambiguity. However, these methods generate attention weights across all attributes and therefore are essentially class-level attention. In

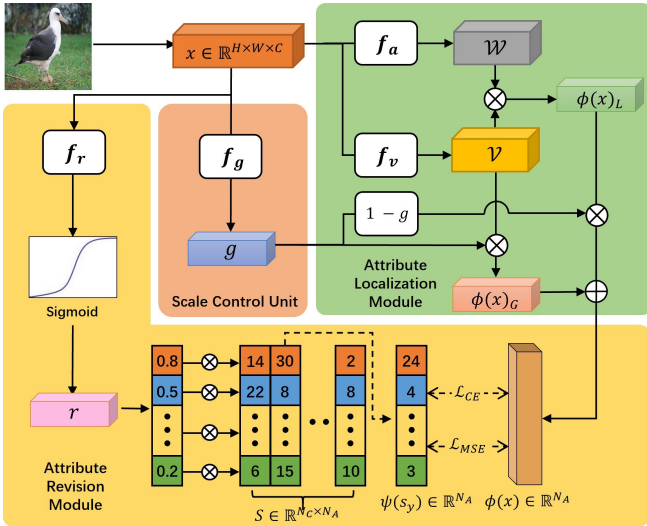


Figure 2: The framework of proposed ALRN, where \otimes denotes element-wise product, and \oplus is addition operation. The attribute Localization Module (green part) tends to localize and evaluate the saliency value of each attribute. The attribute Revision Module (yellow part) produces revision weight for each attribute.

our method, we further fine-grain such an operation into attribute-level, where the weights for each attribute are produced independently. This modification better integrates with the goal of attribute localization to achieve a true attribute revision. Besides, our method first introduces the beneficial role of global features in attention-based methods, which further enhances the ability of our model in extracting attribute features.

3 Proposed Method

In this paper, we propose a novel model called Attribute Localization and Revision Network (ALRN), which consists of two modules. The attribute Localization Module is used to find local regions of an image containing a certain attribute and incorporate the feature of the whole image as a global feature of an attribute. In addition, the proposed Scale Control Unit dynamically controls the network to concentrate on local and global features, which helps the model capture attributes in different scales. Finally, Attribute Revision Module plays a role in independently revising the ground-truth saliency value of each attribute and thus forming new image-level semantics. The whole framework can be found in Figure 2.

3.1 Task Definition and Notations

The seen dataset is denoted as $\mathcal{D}_{tr} = \{(x, y) | x \in \mathcal{X}_s, y \in \mathcal{Y}_s\}$, where \mathcal{X}_s represents a collection of seen visual images, \mathcal{Y}_s are the labels of \mathcal{X}_s . Analogously, the unseen dataset is denoted as $\mathcal{D}_{ts} = \{(x, y) | x \in \mathcal{X}_u, y \in \mathcal{Y}_u\}$, where \mathcal{X}_u represents a collection of unseen visual images, \mathcal{Y}_u are the labels of \mathcal{X}_u . It is worth noting that the seen label space and the unseen label space are disjoint, i.e., $\mathcal{Y}_s \cap \mathcal{Y}_u = \emptyset$. During the training process, semantics $\mathcal{S} \in \mathbb{R}^{N_A \times N_C}$ of all classes are provided, where N_C is the total number of classes and N_A represents the total number of attributes. The semantic

for class i can be written as $s_i = [a_i^1, a_i^2, \dots, a_i^{N_A}]^\top$, where a_i^j means the saliency value of j th attribute with respect to class i . For each image, the feature map obtained through the backbone is represented as $x \in \mathbb{R}^{C \times H \times W}$.

3.2 Attribute Localization and Scale Control

The Attribute Localization Module (ALM) aims at positioning each attribute on an image. It first produces a set of attention weights to localize each attribute. To be specific, a 1×1 convolutional layer f_a is applied to convert the channel dimension of the feature map from C to N_A , then softmax is adopted to encode the attention weight of each attribute:

$$\mathcal{W} = \text{softmax}(f_a(x)), \quad (1)$$

where $\mathcal{W} \in \mathbb{R}^{N_A \times H \times W}$ denotes the attention weights of all attributes. Besides attribute localization, evaluating the saliency value of each attribute is also important for ALM. Another 1×1 convolutional layer f_v is introduced to obtain the saliency map \mathcal{V} . We perform a element-wise product between attention weight map \mathcal{W} and saliency map \mathcal{V} to get the predicted semantic $\phi(x)_L \in \mathbb{R}^{N_A}$:

$$\mathcal{V} = f_v(x), \quad (2)$$

$$\phi_L(x)^n = \sum_{i=1}^H \sum_{j=1}^W \mathcal{W}_{i,j}^n \times \mathcal{V}_{i,j}^n, \quad (3)$$

where $\phi_L(x)^n$ is the predicted saliency value for the n th attribute, $\mathcal{V}_{i,j}^n$ represents the value of the n th attribute with respect to position (i, j) . Note that \mathcal{W} endows different attention weights to different spatial positions, we add the subscript L to $\phi(x)$ to indicate that it represents local feature.

Since holistic attributes are hard to be visually detected on the image. We directly exploit the feature of the whole image to help the model understand them. The global average pooling is incorporated to generate global feature $\phi_G(x) \in \mathbb{R}^{N_A}$:

$$\phi_G(x)^n = \frac{1}{H \times W} \sum_{i=1}^H \sum_{j=1}^W \mathcal{V}_{i,j}^n, \quad (4)$$

where $\phi_G(x)^n$ denotes the saliency value for the n th attribute.

Once local feature $\phi_L(x)$ and global feature $\phi_G(x)$ are obtained, we aggregate them together to acquire the final predicted description $\phi(x)$. To achieve this goal, we propose the Scale Control Unit (SCU) which produces a gate vector $g \in \mathbb{R}^{N_A}$ to help the model adaptively fuse the local or global feature:

$$g^n = \text{sigmoid}\left(\frac{1}{H \times W} \sum_{i=1}^H \sum_{j=1}^W f_g(x)_{i,j}^n\right), \quad (5)$$

where f_g denotes 1×1 convolutional layer, superscript n means the value at n th channel dimension, and subscript i, j stands for the value at spatial position (i, j) . The final predicted description $\phi(x) \in \mathbb{R}^{N_A}$ is generated as follows:

$$\phi(x) = g \times \phi_L(x) + (1 - g) \times \phi_G(x). \quad (6)$$

The predicted semantic description $\phi(x)$ incorporates both local and global information, making it able to evaluate the

saliency value of both local and holistic attributes. Traditionally, $\phi(x)$ is used to align with the corresponding class-level semantic description. However, as we illustrated before, it ignores the differences between images within the same class. Therefore, we propose Attribute Revision Module to alleviate this problem.

3.3 Attribute Revision

Similar to ALM, the Attribute Revision Module (ARM) also need to obtain the feature of each attribute independently to let the model know how to revise the saliency value of each attribute. The revision vector $r \in \mathbb{R}^{N_A}$ is calculated as follows:

$$r^n = \text{sigmoid}\left(\frac{1}{H \times W} \sum_{i=1}^H \sum_{j=1}^W f_r(x)_{i,j}^n\right), \quad (7)$$

where f_r denotes 1×1 convolutional layer, superscript n means the value at n th channel dimension, and subscript i, j stands for the value at spatial position (i, j) . A low weight value means the corresponding attribute saliency value should be suppressed. Conversely, a weight close to one means that the corresponding saliency value should be retained.

Based on the illustration above, r does a element-wise product with each semantic vector $s \in \mathbb{R}^{N_A}$ in \mathcal{S} :

$$\psi_x(s_i) = [r^1 \times a_i^1, r^2 \times a_i^2, \dots, r^{N_A} \times a_i^{N_A}]^\top, \quad (8)$$

where $\psi_x(s_i)$ means the image-level semantic vector for class i with respect to image x , r^i represents the revision weight for i th attribute, and a_j^i is the real saliency value of the i th attribute for class j .

3.4 Training Algorithm

Once predicted semantic description $\phi(x)$ and image-level semantic vectors $\psi_x(s)$ are obtained, two loss functions are introduced to train the model. The first one is a cross-entropy loss which pushes $\phi(x)$ close to the target semantic vector $\psi_x(s_y)$ and far away from semantic vectors belonging to other classes:

$$\mathcal{L}_{CE} = -\frac{1}{N_B} \sum_{i=1}^{N_B} \log \frac{\tau \exp(\cos(\phi(x_i), \psi_x(s_y)))}{\sum_{\hat{y} \in \mathcal{Y}_s} \exp(\tau \cos(\phi(x_i), \psi_x(s_{\hat{y}})))}, \quad (9)$$

where τ is a scaling coefficient, N_B represents the size of a mini-batch, $\psi_x(s_{\hat{y}})$ denotes the image-level semantic description of class \hat{y} with respect to the i th image in mini-batch, and $\cos(\cdot)$ means cosine similarity.

It is worth noting that \mathcal{L}_{CE} acts as a class-level alignment between output features and semantics of different classes. However, since our model predicts the saliency value of each attribute independently, it is essential to directly align the attribute feature. Therefore, a mean squared error loss function is applied to serve as an auxiliary to \mathcal{L}_{CE} , which is an attribute-level alignment between the values of $\phi(x)$ and $\psi_x(s)$ in each dimension:

$$\mathcal{L}_{MSE} = \frac{1}{N_B} \sum_{i=1}^{N_B} \|\phi(x_i) - \psi_x(s_y)\|_2^2. \quad (10)$$

Therefore, the complete loss function can be written as:

$$\mathcal{L} = \mathcal{L}_{CE} + \lambda \mathcal{L}_{MSE}. \quad (11)$$

where λ is a manually controlled hyper-parameter.

The training algorithm contains two stages, i.e, the kernel pretraining stage and the end-to-end training stage. During the kernel pretraining stage, only four sets of convolutional kernels will be trained. The number of training epoch N_{pre} for this stage is a hyper-parameter tuned manually. After N_{pre} training epochs, the training strategy converts to end-to-end training updating the parameter of the whole network simultaneously.

3.5 Prediction Method

In conventional ZSL, test images are only from unseen classes, so the classification space is limited to \mathcal{Y}_u . The prediction results are calculated as follows:

$$\tilde{y} = \underset{\hat{y} \in \mathcal{Y}_u}{\text{argmax}} \cos(\phi(x), \psi(s_{\hat{y}})), \quad (12)$$

where \tilde{y} is the predicted label for input image x and $s_{\hat{y}}$ represents the semantic vector of class \hat{y} . For GZSL, to prevent the model from overly concentrating on seen class, the calibration stacking mechanism [Chao *et al.*, 2016] is applied to reduce prediction scores on seen classes.

$$\tilde{y} = \underset{\hat{y} \in \mathcal{Y}_s \cup \mathcal{Y}_u}{\text{argmax}} (\tau \cos(\phi(x), \psi_x(s_{\hat{y}})) - \mu \mathbb{I}[\hat{y} \in \mathcal{Y}_s]), \quad (13)$$

where $\mathbb{I}[\cdot]$ is an indication function whose value will be one if $\hat{y} \in \mathcal{Y}_s$, μ is a reduction factor needing to be tuned manually, and τ is the same hyper-parameter in Eq. 9.

4 Experiments

4.1 Experimental Setup

Benchmarks We evaluate our model on three popular benchmarks in the ZSL field. Animal with Attributes 2 (AWA2) [Xian *et al.*, 2018a] is a dataset describing different kinds of animals, which contains 37,322 images belonging to 40 seen classes and 10 unseen classes with each class represented by 50 attributes. Caltech-UCSD-Birds-200-2011 (CUB) [Welinder *et al.*, 2010] consists of 11,788 bird images from 200 classes where each class has 312 attributes. The number of seen and unseen classes for the CUB dataset is set as 150 and 50, respectively. SUN attribute database (SUN) [Patterson and Hays, 2012] is composed of 14,340 images from 717 classes, with 645 seen classes and 72 unseen classes. Each class in SUN can be described by a 102-dimension semantic vector. In terms of data split, we follow the seen/unseen split proposed in [Xian *et al.*, 2018a] to validate the performance of our method.

Evaluation Metric The metrics for conventional ZSL and GZSL are different. For conventional ZSL, the test set only consists of unseen classes, the metric is the per-class Top-1 prediction accuracy for predicting unseen classes, which is denoted as $\mathbf{T1}$. For GZSL, since the test set contains both seen and unseen classes, two per-class Top-1 prediction accuracy \mathbf{S} and \mathbf{U} can be calculated, where \mathbf{S} represents seen accuracy and \mathbf{U} means unseen accuracy. To comprehensively

	Methods	Venues	CUB			SUN			AWA2		
			S	U	H	S	U	H	S	U	H
Projection	DeViSE [Frome <i>et al.</i> , 2013]	NIPS’13	53.0	23.8	32.8	16.9	20.9	23.1	74.7	17.1	27.8
	SJE [Akata <i>et al.</i> , 2015b]	CVPR’15	59.2	23.5	33.6	30.5	14.7	19.8	73.9	8.0	14.4
	DCN [Liu <i>et al.</i> , 2018]	NIPS’18	60.7	28.4	38.7	37.0	25.5	30.2	—	—	—
	TCN [Jiang <i>et al.</i> , 2019]	ICCV’19	48.1	33.3	39.4	18.5	30.9	23.1	72.8	52.1	60.7
	CADA-VAE [Schonfeld <i>et al.</i> , 2019]	CVPR’19	53.5	51.6	52.4	35.7	47.2	40.6	75.0	55.8	63.9
	Li <i>et al.</i> [Li <i>et al.</i> , 2019b]	ICCV’19	47.6	47.4	47.5	42.8	36.3	39.3	81.4	56.4	66.7
	AGZSL [Chou <i>et al.</i> , 2020]	ICLR’21	41.4	49.7	45.2	29.9	40.2	34.3	78.9	65.1	<u>71.3</u>
	TDCSS [Feng <i>et al.</i> , 2022]	CVPR’22	62.8	44.2	51.9	—	—	—	74.9	59.2	66.1
	VGSE [Xu <i>et al.</i> , 2022]	CVPR’22	24.1	45.7	31.5	25.5	35.7	29.8	45.7	66.7	54.2
Generation	f-CLSWGAN [Xian <i>et al.</i> , 2018b]	CVPR’18	43.7	57.7	49.7	36.6	42.6	39.4	57.9	61.4	59.6
	LisGAN [Li <i>et al.</i> , 2019a]	CVPR’19	57.9	46.5	51.6	37.8	42.9	40.2	—	—	—
	LsrGAN [Vyas <i>et al.</i> , 2020]	ECCV’20	59.1	48.1	53.0	37.7	44.8	40.9	74.6	54.6	63.0
	SAGAN [Tang <i>et al.</i> , 2022]	TNNLS’20	59.5	45.3	51.4	29.8	44.6	35.8	84.2	55.9	67.2
	CE-GZSL [Han <i>et al.</i> , 2021]	CVPR’21	66.8	63.9	65.3	<u>38.6</u>	<u>48.8</u>	43.1	78.6	63.1	70.0
	FREE [Chen <i>et al.</i> , 2021b]	ICCV’21	59.9	55.7	57.7	37.2	47.4	<u>41.7</u>	75.4	60.4	67.1
Attention	LFGAA [Liu <i>et al.</i> , 2019]	CVPR’19	79.6	43.4	56.2	34.9	20.8	26.1	<u>90.3</u>	50.0	64.4
	AREN [Xie <i>et al.</i> , 2019]	CVPR’19	<u>78.7</u>	38.9	52.1	38.8	19.0	25.5	92.9	15.6	26.7
	DAZLE [Huynh and Elhamifar, 2020]	CVPR’20	<u>56.7</u>	59.6	58.1	24.3	52.3	33.2	75.7	60.3	67.1
	APN [Xu <i>et al.</i> , 2020]	NIPS’20	69.3	<u>65.3</u>	67.2	34.0	41.9	37.6	78.0	56.5	65.5
	GEM-ZSL [Liu <i>et al.</i> , 2021]	CVPR’21	77.1	64.8	<u>70.4</u>	35.7	38.1	36.9	77.5	64.8	70.6
	ALRN	Ours	77.6	68.2	72.6	36.4	46.7	40.9	81.3	64.8	72.1

Table 1: GZSL results comparison on CUB, SUN, and AWA2. The best results and second best results are in **bold** and underline, respectively.

Methods	CUB	SUN	AWA2
SP-AEN [Chen <i>et al.</i> , 2018]	55.4	59.2	58.5
AREN [Xian <i>et al.</i> , 2018b]	71.8	60.6	67.9
SGMA [Zhu <i>et al.</i> , 2019]	71.0	-	68.8
DAZLE [Huynh and Elhamifar, 2020]	66.0	59.4	67.9
APN [Xu <i>et al.</i> , 2020]	72.0	61.6	58.4
TransZero [Chen <i>et al.</i> , 2021a]	<u>76.8</u>	<u>65.6</u>	70.1
MSDN [Chen <i>et al.</i> , 2022]	76.1	65.8	70.1
ALRN	77.2	65.1	69.7

Table 2: Per-class Top-1 accuracies comparison under conventional ZSL on CUB, SUN and AWA2 among attention-based methods. The best results and second best results are labeled in **bold** and underline, respectively.

evaluate the accuracies on both seen and unseen data, the harmonic mean $H = (2 \times S \times U) / (S + U)$ is computed to provide a unified evaluation protocol for the GZSL setting. ZSL task seeks balanced predictive performance on seen and unseen classes, so the comparison on harmonic mean H is better than simply comparing seen or unseen accuracy.

Experimental Details The backbone of our proposed ALRN is a ResNet101 [He *et al.*, 2016] pre-trained on ImageNet-1K. The epoch number N_{pre} for training four different sets of 1×1 convolutional layers, i.e., f_a , f_v , f_r , f_g , is set as one for AWA2, five for CUB and SUN. The scaling coefficient τ is set as 35 for CUB, as well as 20 for SUN and AWA2. The reduction factor μ is set as 1.5 for SUN, 2.35 for CUB, and 3.9 for AWA2. The weight loss λ is set

as one for CUB and AWA2, 1.5 for SUN. During the training process, an SGD with momentum optimizer is applied to update parameters, where the learning rate is set as 0.001, the momentum value is set as 0.9, and weight decay is set as 0.00001. Episode-training strategy [Wang *et al.*, 2021] is adopted which randomly samples images from 16 classes with two images for each class as a mini-batch. We iterate 300 mini-batch in an epoch and train the model 20 epochs for all three datasets.

4.2 Comparison with Previous Works

Generalized Zero-Shot Learning For the GZSL setting, our ALRN produces the best harmonic mean 72.6% on CUB, which is 2.2% higher than the second best result 70.4% obtained by GEM-ZSL [Liu *et al.*, 2021]. Also, our method gets 72.1% on AWA2, which is 0.8% higher than the result obtained by AGZSL [Chou *et al.*, 2020]. For the SUN dataset, the contents of images are complex scenes rather than concrete objects, it is difficult for the model to analyze the detailed information within each image. In such a case, it is challenging for attention-based methods to localize attributes on the SUN dataset. Nevertheless, our ALRN still achieves the highest harmonic mean 40.9% on the SUN dataset, leading by 3.3% harmonic mean with the second best harmonic mean produced by APN [Xu *et al.*, 2020], which is also the most representative method in attention-based methods. In general, benefiting from balanced performance on both seen and unseen classes, our method achieves the highest harmonic mean on two datasets, i.e., CUB and AWA2. Also, the competitive performance of SUN supports the effectiveness

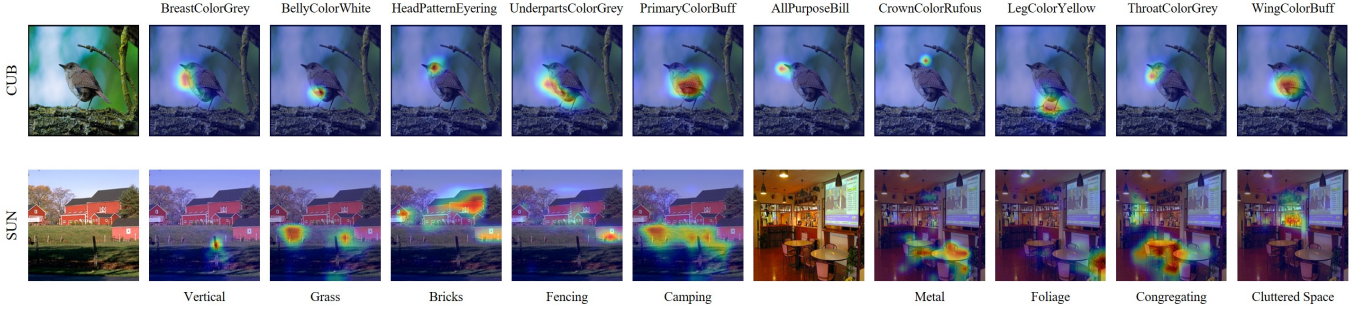


Figure 3: The visualization results of attention maps. For the CUB dataset, one randomly selected image and ten attention maps are shown. For the SUN dataset, two randomly selected images and nine attention maps are exhibited.

Algorithm	SUN			AWA2		
	<i>S</i>	<i>U</i>	<i>H</i>	<i>S</i>	<i>U</i>	<i>H</i>
ALRN w/o ARM & SCU	29.2	52.7	37.6	80.4	59.3	68.3
ALRN w/o SCU	30.2	51.1	38.0	79.7	60.8	69.0
ALRN w/o \mathcal{L}_{MSE}	32.3	49.7	39.2	84.9	58.3	69.1
ALRN w/o global feature	35.0	48.3	40.5	83.0	56.3	67.1
ALRN (full)	36.4	46.7	40.9	81.3	64.8	72.1

Table 3: Ablation studies under different model structures and training algorithms in SUN and AWA2. The best results are in **bold**.

of integrating global feature and attribute revision mechanism in our method.

Conventional Zero-Shot Learning As shown in Table 2, our ALRN gets the best Top-1 accuracy ($T1$) on CUB, where the value of $T1$ is 0.4% higher than the best result obtained by TransZero [Chen *et al.*, 2021a]. Also, our method achieves the second best $T1$ on AWA2, which is only 0.4% lower than the highest result produced by TransZero [Chen *et al.*, 2021a] and MSDN [Chen *et al.*, 2022]. It is worth mentioning that ALRN gets competitive $T1$ on SUN, where it is only 0.7% lower than the best accuracy produced by MSDN [Chen *et al.*, 2022], and it surpasses 3.5% than representative method APN [Xu *et al.*, 2020].

4.3 Ablation Studies

Model Structure and Training Algorithm We conduct ablation studies to demonstrate the effectiveness of each module by training the model under different structures in Table 3. It is worth noting that if SCU is deleted, the global and local features will be simply averaged together, and if the ARM is deleted, the output feature of ALRN will directly align with class-level semantics. As we can see from Table 3, the removal of the global feature leads to a 0.4% and 5.0% harmonic mean degradation on SUN and AWA2, respectively. Analogously, the deletion of SCU leads 2.9% and 3.1% harmonic mean reduction on two datasets. Besides the experiments about different model structures, the effectiveness of attribute-level alignment loss, i.e., \mathcal{L}_{MSE} is also worth investigating, where the model only obtains 39.2% on SUN, and 69.1% on AWA2. In summary, the ablation study results demonstrates that each network module is indispensable in our approach.

Mechanism	SUN			AWA2		
	<i>S</i>	<i>U</i>	<i>H</i>	<i>S</i>	<i>U</i>	<i>H</i>
ALRN w/o ARM	29.2	52.7	37.6	80.4	59.3	68.3
ALRN w/ softmax	31.6	50.1	38.8	81.6	61.8	70.3
ALRN w/ sigmoid	36.4	46.7	40.9	81.3	64.8	72.1

Table 4: Ablation studies under three different revision mechanisms in SUN and AWA2. The best results are in **bold**.

Revision Mechanism We also explore the performance under different revision operations in Table 4. The model without revision, which is achieved by abandoning ARM, drives the model a 3.3% and 3.8% harmonic mean decrease on SUN and AWA2. Then, we replace the sigmoid in Eq. 7 with softmax, which injects competence between different attributes during the revision weights calculation process. The model with softmax obtains 38.8% on SUN and 70.3% on AWA2, which are 2.1% and 1.8% lower than the harmonic mean obtained by the model trained with sigmoid. This supports that our proposed attribute-level revision mechanism is more suitable for attention-based approaches.

4.4 Visualization Results

Visualization of Attention Maps We present the attention visualization results of ALM in Figure 3. The ALM performs outstanding ability in locating CUB attributes, where the results can be found in the first row of Figure 3. In the second row, we present nine attention maps of two images from the SUN dataset. We can find that ALRN correctly recognizes the wooden stick as vertical, and a large area of grass as camping. Furthermore, our ALRN accurately identifies the place where tables and chairs are gathered as congregating and the bar counter as a cluttered space in the last two attention maps in the second row. In summary, although attributes in the SUN dataset are more semantically related to the image, we can still observe excellent attributes localization skills of our model.

Visualization of Revised Semantics For our proposed attribute revision, two concerns may arise. First, the network will produce identical revision weights to all attributes, causing the revised semantics to be the same as the original semantics. Second, attribute revision will break the distribution

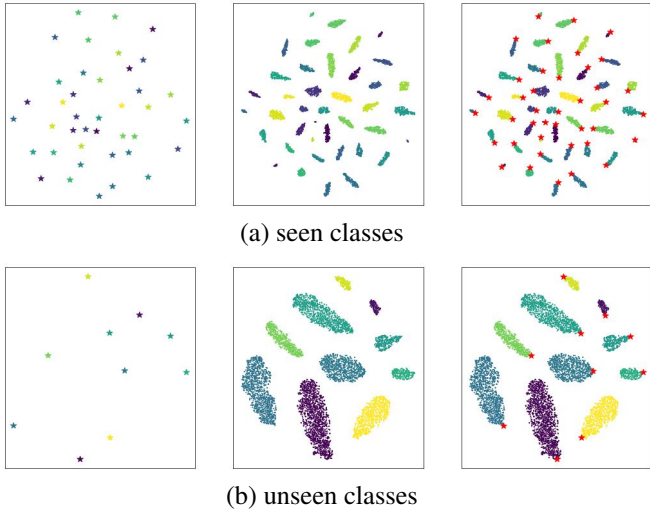


Figure 4: The first two subfigures in each row represent original and revised semantics. The last subfigure combines two previous subfigures, where red stars stand for original semantics.

structure of the original semantics, leading to a less robust model. To deal with these concerns, we visualize the distribution of original and revised semantics to explore the distribution of semantics after conducting attribute revision in Figure 4. Samples from both seen and unseen classes in the test set of AWA2 are fed into the network, then the revised semantics which correspond to the labels are visualized via the t-sne algorithm [Maaten and Hinton, 2008]. As we can see, the revised semantics of different classes exhibit diverging distribution, which starts at the original semantics and diverges in one direction. Also, these revised semantics show good clustering rather than mixed together even for unseen classes. This phenomenon demonstrates our model indeed injects the intra-class variation from the perspective of revising the learning objective and such a revision mechanism is robust enough to prevent semantic features from mixed together and further collapsing.

4.5 Hyper-parameter Analysis

Effects of Pretraining Epochs We vary the parameter N_{pre} by selecting one of the exact number in $\{2, 3, 4, 5, 6\}$ on both SUN and AWA2. As we can see from two subfigures in Figure 5 (1), the model obtains the highest harmonic mean 72.6% on CUB and 40.9% on SUN when N_{pre} is set as 5. This result demonstrates that it is necessary to first adapt four sets of convolutional kernels with the pre-trained backbone, then conduct end-to-end training with the whole network.

Effects of Scaling Coefficient For the effects of scaling parameter τ , which are exhibited in two subfigures of Figure 5 (2), our model gets the highest H value 72.6% on CUB when τ is set as 20 and gets the best H value 40.9% when τ equals 35. Since the attributes in CUB are local attributes that are easily captured and recognized, a relatively low scaling coefficient is enough to distinguish different classes. However, SUN is a scene dataset where image samples are hard to un-

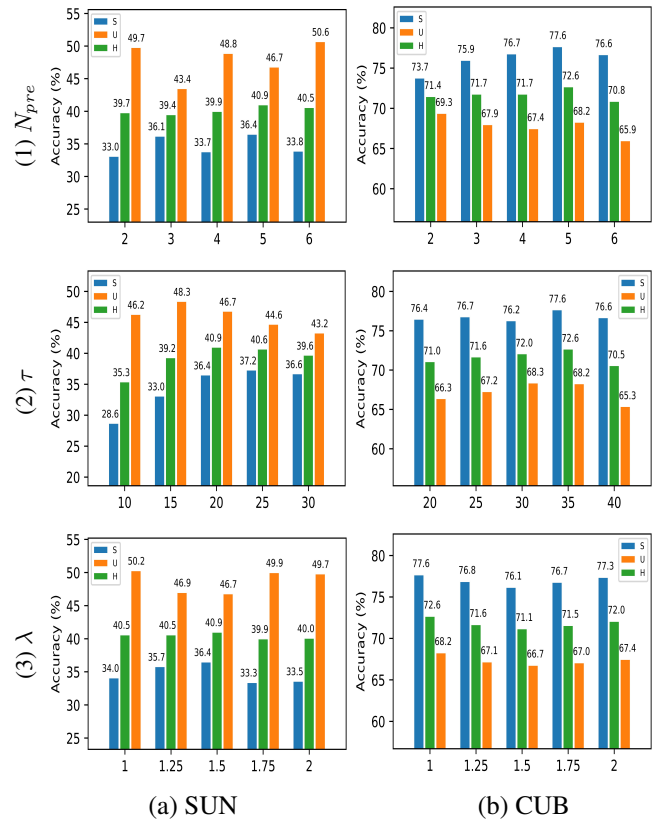


Figure 5: The effect of N_{pre} , τ , and λ on SUN and CUB.

derstand, the model needs a larger scaling coefficient to separate the prediction of different samples.

Effects of Loss Weight The weight hyper-parameter directly determines how much attribute alignment loss \mathcal{L}_{MSE} is performed in ALRN. From the third row of Figure 5, we find that ALRN performs best on SUN when λ is set as 1.5 and gets the highest harmonic mean on CUB when λ is set as 1. The difficulty of identifying attributes in SUN requires ALRN to spend more effort on aligning the saliency values of each attribute rather than on the overall semantics.

5 Conclusion

In this work, we propose Attribute Localization and Revision Network (ALRN), which tackles the deficiencies of the previous attention-based works that ignore global features and intra-class attribute variation. Experimental results on three widely used benchmarks have shown a significant ability in zero-shot prediction and attribute localization. In future works, we will explore a better way to help the model understand holistic attributes. Also, we will attempt to use vision transformers [Dosovitskiy *et al.*, 2020] as our backbone to achieve attribute localization and revision.

References

[Akata *et al.*, 2015a] Zeynep Akata, Florent Perronnin, Zaid Harchaoui, and Cordelia Schmid. Label-embedding for

image classification. *IEEE Trans. Pattern Anal. Mach. Intell.*, 38(7):1425–1438, 2015.

[Akata *et al.*, 2015b] Zeynep Akata, Scott Reed, Daniel Walther, Honglak Lee, and Bernt Schiele. Evaluation of output embeddings for fine-grained image classification. In *Proc. IEEE Conf. Comput. Vis. Pattern Recog.*, pages 2927–2936, Boston, MA, Jun. 2015.

[Chao *et al.*, 2016] Wei-Lun Chao, Soravit Changpinyo, Boqing Gong, and Fei Sha. An empirical study and analysis of generalized zero-shot learning for object recognition in the wild. In *Proc. Eur. Conf. Comput. Vis.*, pages 52–68, Amsterdam, Netherland, Oct. 2016.

[Chen *et al.*, 2018] Long Chen, Hanwang Zhang, Jun Xiao, Wei Liu, and Shih-Fu Chang. Zero-shot visual recognition using semantics-preserving adversarial embedding networks. In *Proc. IEEE Conf. Comput. Vis. Pattern Recog.*, pages 1043–1052, Salt Lake City, UT, Jun. 2018.

[Chen *et al.*, 2021a] Shiming Chen, Ziming Hong, Yang Liu, Guo-Sen Xie, Baigui Sun, Hao Li, Qinmu Peng, Ke Lu, and Xinge You. Transzero: Attribute-guided transformer for zero-shot learning. 2021. [Online], Available: <http://arxiv.org/abs/2112.01683>.

[Chen *et al.*, 2021b] Shiming Chen, Wenjie Wang, Beihao Xia, Qinmu Peng, Xinge You, Feng Zheng, and Ling Shao. Free: Feature refinement for generalized zero-shot learning. In *Proc. IEEE Int. Conf. Comput. Vis.*, pages 122–131, Jun. 2021.

[Chen *et al.*, 2022] Shiming Chen, Ziming Hong, Guo-Sen Xie, Wenhan Yang, Qinmu Peng, Kai Wang, Jian Zhao, and Xinge You. Msdn: Mutually semantic distillation network for zero-shot learning. In *Proc. IEEE Conf. Comput. Vis. Pattern Recog.*, pages 7612–7621, New Orleans, LA, Jun. 2022.

[Chou *et al.*, 2020] Yu-Ying Chou, Hsuan-Tien Lin, and Tyng-Luh Liu. Adaptive and generative zero-shot learning. In *Proc. Int. Conf. Learn. Represent.*, Apr. 2020.

[Dosovitskiy *et al.*, 2020] Alexey Dosovitskiy, Lucas Beyer, Alexander Kolesnikov, Dirk Weissenborn, Xiaohua Zhai, Thomas Unterthiner, Mostafa Dehghani, Matthias Minderer, Georg Heigold, Sylvain Gelly, et al. An image is worth 16x16 words: Transformers for image recognition at scale. 2020. [Online], Available: <http://arxiv.org/abs/2010.11929>.

[Feng *et al.*, 2022] Yaogong Feng, Xiaowen Huang, Pengbo Yang, Jian Yu, and Jitao Sang. Non-generative generalized zero-shot learning via task-correlated disentanglement and controllable samples synthesis. In *Proc. IEEE Conf. Comput. Vis. Pattern Recog.*, pages 9346–9355, New Orleans, LA, Jun. 2022.

[Frome *et al.*, 2013] Andrea Frome, Greg Corrado, Jonathon Shlens, Samy Bengio, Jeffrey Dean, Marc’Aurelio Ranzato, and Tomas Mikolov. Devise: A deep visual-semantic embedding model. In *Proc. Adv. Neural Inf. Process. Syst.*, pages 2121–2129, Lake Tahoe, NV, Dec. 2013.

[Goodfellow *et al.*, 2014] Ian Goodfellow, Jean Pouget-Abadie, Mehdi Mirza, Bing Xu, David Warde-Farley, Sherjil Ozair, Aaron Courville, and Yoshua Bengio. Generative adversarial nets. In *Proc. Adv. Neural Inf. Process. Syst.*, pages 2672–2680, Montréal, Québec, Canada, Dec. 2014.

[Han *et al.*, 2020] Zongyan Han, Zhenyong Fu, and Jian Yang. Learning the redundancy-free features for generalized zero-shot object recognition. In *Proc. IEEE Conf. Comput. Vis. Pattern Recog.*, pages 12865–12874, Seattle, WA, Jun. 2020.

[Han *et al.*, 2021] Zongyan Han, Zhenyong Fu, Shuo Chen, and Jian Yang. Contrastive embedding for generalized zero-shot learning. In *Proc. IEEE Conf. Comput. Vis. Pattern Recog.*, pages 2371–2381, Jun. 2021.

[He *et al.*, 2016] Kaiming He, Xiangyu Zhang, Shaoqing Ren, and Jian Sun. Deep residual learning for image recognition. In *Proc. IEEE Conf. Comput. Vis. Pattern Recog.*, pages 770–778, Las Vegas, NV, Jun. 2016.

[Huynh and Elhamifar, 2020] Dat Huynh and Ehsan Elhamifar. Fine-grained generalized zero-shot learning via dense attribute-based attention. In *Proc. IEEE Conf. Comput. Vis. Pattern Recog.*, pages 4483–4493, Seattle, WA, Jun. 2020.

[Jiang *et al.*, 2019] Huajie Jiang, Ruiping Wang, Shiguang Shan, and Xilin Chen. Transferable contrastive network for generalized zero-shot learning. In *Proc. IEEE Int. Conf. Comput. Vis.*, pages 9765–9774, Seoul, Korea, Oct. 2019.

[Kingma and Welling, 2014] Diederik P Kingma and Max Welling. Auto-encoding variational bayes. 2014. [Online], Available: <http://arxiv.org/abs/1312.6114>.

[Lampert *et al.*, 2009] Christoph H Lampert, Hannes Nickisch, and Stefan Harmeling. Learning to detect unseen object classes by between-class attribute transfer. In *Proc. IEEE Conf. Comput. Vis. Pattern Recog.*, pages 951–958, Miami, FL, Jun. 2009.

[Li *et al.*, 2019a] Jingjing Li, Mengmeng Jing, Ke Lu, Zhengming Ding, Lei Zhu, and Zi Huang. Leveraging the invariant side of generative zero-shot learning. In *Proc. IEEE Conf. Comput. Vis. Pattern Recog.*, pages 7402–7411, Long Beach, CA, Jun. 2019.

[Li *et al.*, 2019b] Kai Li, Martin Renqiang Min, and Yun Fu. Rethinking zero-shot learning: A conditional visual classification perspective. In *Proc. IEEE Int. Conf. Comput. Vis.*, pages 3583–3592, Seoul, Korea, Oct. 2019.

[Liu *et al.*, 2018] Shichen Liu, Mingsheng Long, Jianmin Wang, and Michael I Jordan. Generalized zero-shot learning with deep calibration network. In *Proc. Adv. Neural Inf. Process. Syst.*, pages 2005–2015, Montréal, Québec, Canada, Dec. 2018.

[Liu *et al.*, 2019] Yang Liu, Jishun Guo, Deng Cai, and Xiaofei He. Attribute attention for semantic disambiguation in zero-shot learning. In *Proc. IEEE Int. Conf. Comput. Vis.*, pages 6698–6707, Seoul, Korea, Oct. 2019.

[Liu *et al.*, 2021] Yang Liu, Lei Zhou, Xiao Bai, Yifei Huang, Lin Gu, Jun Zhou, and Tatsuya Harada. Goal-oriented gaze estimation for zero-shot learning. In *Proc. IEEE Conf. Comput. Vis. Pattern Recog.*, Jun. 2021.

[Maaten and Hinton, 2008] Laurens Van Der Maaten and Geoffrey Hinton. Visualizing data using t-sne. *Journal of Machine Learning Research*, 9:2579–2605, 2008.

[Mishra *et al.*, 2018] Ashish Mishra, Shiva Krishna Reddy, Anurag Mittal, and Hema A Murthy. A generative model for zero shot learning using conditional variational autoencoders. In *Proc. IEEE Conf. Comput. Vis. Pattern Recog. Worksh.*, pages 2188–2196, Salt Lake City, UT, Jun. 2018.

[Narayan *et al.*, 2020] Sanath Narayan, Akshita Gupta, Fahad Shahbaz Khan, Cees GM Snoek, and Ling Shao. Latent embedding feedback and discriminative features for zero-shot classification. In *Proc. Eur. Conf. Comput. Vis.*, pages 479–495, Glasgow, UK, Aug. 2020.

[Patterson and Hays, 2012] Genevieve Patterson and James Hays. Sun attribute database: Discovering, annotating, and recognizing scene attributes. In *Proc. IEEE Conf. Comput. Vis. Pattern Recog.*, pages 2751–2758, Providence, RI, Jun. 2012.

[Schonfeld *et al.*, 2019] Edgar Schonfeld, Sayna Ebrahimi, Samarth Sinha, Trevor Darrell, and Zeynep Akata. Generalized zero-and few-shot learning via aligned variational autoencoders. In *Proc. IEEE Conf. Comput. Vis. Pattern Recog.*, pages 8247–8255, Long Beach, CA, Jun. 2019.

[Tang *et al.*, 2022] Chenwei Tang, Zhenan He, Yunxia Li, and Jiancheng Lv. Zero-shot learning via structure-aligned generative adversarial network. *IEEE Trans. Neural Netw. Learn. Syst.*, 33(11):6749–6762, 2022.

[Verma *et al.*, 2018] Vinay Kumar Verma, Gundeep Arora, Ashish Mishra, and Piyush Rai. Generalized zero-shot learning via synthesized examples. In *Proc. IEEE Conf. Comput. Vis. Pattern Recog.*, pages 4281–4289, Salt Lake City, UT, Jun. 2018.

[Vyas *et al.*, 2020] Maunil R Vyas, Hemanth Venkateswara, and Sethuraman Panchanathan. Leveraging seen and unseen semantic relationships for generative zero-shot learning. In *Proc. Eur. Conf. Comput. Vis.*, pages 70–86, Glasgow, UK, Aug. 2020.

[Wang *et al.*, 2021] Ziyang Wang, Yunhao Gou, Jingjing Li, Yu Zhang, and Yang Yang. Region semantically aligned network for zero-shot learning. In *Int. Conf. Inf. Knowledge Manage.*, pages 2080–2090, Queensland, Australia, Nov. 2021.

[Welinder *et al.*, 2010] P. Welinder, S. Branson, T. Mita, C. Wah, F. Schroff, S. Belongie, and P. Perona. Caltech-ucsd birds 200. Technical Report CNS-TR-2010-001, California Institute of Technology, Pasadena, CA, 2010.

[Xian *et al.*, 2018a] Yongqin Xian, Christoph H Lampert, Bernt Schiele, and Zeynep Akata. Zero-shot learning—a comprehensive evaluation of the good, the bad and the ugly. *IEEE Trans. Pattern Anal. Mach. Intell.*, 41(9):2251–2265, 2018.

[Xian *et al.*, 2018b] Yongqin Xian, Tobias Lorenz, Bernt Schiele, and Zeynep Akata. Feature generating networks for zero-shot learning. In *Proc. IEEE Conf. Comput. Vis. Pattern Recog.*, pages 5542–5551, Salt Lake City, UT, Jun. 2018.

[Xian *et al.*, 2019] Yongqin Xian, Saurabh Sharma, Bernt Schiele, and Zeynep Akata. f-vaegan-d2: A feature generating framework for any-shot learning. In *Proc. IEEE Conf. Comput. Vis. Pattern Recog.*, pages 10275–10284, Long Beach, CA, Jun. 2019.

[Xie *et al.*, 2019] Guo-Sen Xie, Li Liu, Xiaobo Jin, Fan Zhu, Zheng Zhang, Jie Qin, Yazhou Yao, and Ling Shao. Attentive region embedding network for zero-shot learning. In *Proc. IEEE Conf. Comput. Vis. Pattern Recog.*, pages 9384–9393, Long Beach, CA, Jun. 2019.

[Xie *et al.*, 2022] Guo-Sen Xie, Zheng Zhang, Guoshuai Liu, Fan Zhu, Li Liu, Ling Shao, and Xuelong Li. Generalized zero-shot learning with multiple graph adaptive generative networks. *IEEE Trans. Neural Netw. Learn. Syst.*, 33(7):2903–2915, 2022.

[Xu *et al.*, 2020] Wenjia Xu, Yongqin Xian, Jiuniu Wang, Bernt Schiele, and Zeynep Akata. Attribute prototype network for zero-shot learning. In *Proc. Adv. Neural Inf. Proces. Syst.*, pages 21969–21980, Dec. 2020.

[Xu *et al.*, 2022] Wenjia Xu, Yongqin Xian, Jiuniu Wang, Bernt Schiele, and Zeynep Akata. Vgse: Visually-grounded semantic embeddings for zero-shot learning. In *Proc. IEEE Conf. Comput. Vis. Pattern Recog.*, pages 9316–9325, New Orleans, LA, Jun. 2022.

[Yang *et al.*, 2021] Shiqi Yang, Kai Wang, Luis Herranz, and Joost van de Weijer. On implicit attribute localization for generalized zero-shot learning. *IEEE Signal Processing Letters*, 28:872–876, 2021.

[Yu *et al.*, 2020] Yunlong Yu, Zhong Ji, Jungong Han, and Zhongfei Zhang. Episode-based prototype generating network for zero-shot learning. In *Proc. IEEE Conf. Comput. Vis. Pattern Recog.*, pages 14035–14044, Seattle, WA, Jun. 2020.

[Zhu *et al.*, 2019] Yizhe Zhu, Jianwen Xie, Zhiqiang Tang, Xi Peng, and Ahmed Elgammal. Semantic-guided multi-attention localization for zero-shot learning. In *Proc. Adv. Neural Inf. Proces. Syst.*, pages 14290–15070, Vancouver, BC, Canada, Dec. 2019.